ACS SENSORS

pubs.acs.org/acssensors

Article

Electrochemiluminescence Biosensor for Nucleolin Imaging in a Single Tumor Cell Combined with Synergetic Therapy of Tumor

Wanxia Gao, Yong Liu, Huairong Zhang,* and Zonghua Wang*

Cite This: *ACS Sens.* 2020, 5, 1216–1222

Read Online

ACCESS | Metrics & More | Article Recommendations | Supporting Information

ABSTRACT: Nucleolin, a nuclear biological multifunctional protein, plays significant roles in modulating the proliferation, survival, and apoptosis of tumor cells. Different from the traditional electrochemiluminescence (ECL) method, a new ECL biosensor was built to perform ECL imaging of nucleolin in a single HeLa cell with high sensitivity and throughput. Briefly, mesoporous silica nanoparticles (MSN) loaded with doxorubicin (DOX) and phorbol 12-myristate 13-acetate (PMA) were used as drug carriers and could be specifically opened by nucleolin in a HeLa cell. PMA then induced the HeLa cell to produce reactive oxygen species (ROS) and realized ECL imaging of nucleolin. After that, ROS could damage DNA and proteins of the tumor cell and DOX could induce the apoptosis of HeLa cells by inhibiting genetic material, nucleic acid, synthesis. HeLa cells were then efficiently killed by DOX and ROS in a synergetic pathway. Herein, a new ECL biosensor for ECL imaging of nucleolin in a single HeLa cell and synergetic tumor therapy was built.

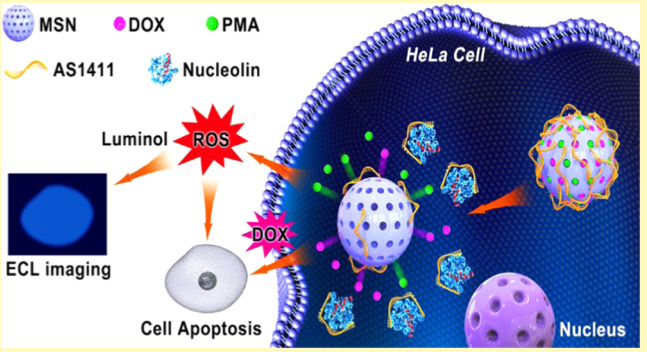

KEYWORDS: *electrochemiluminescence biosensor, nucleolin, single-cell detection, silica nanoparticles, synergetic apoptosis*

Nucleolin, as one of the most abundant proteins in the nucleolus, was also found in the cytoplasm and on the cell membrane.[1−4] It has been confirmed that nucleolin plays significant roles in modulating the proliferation, survival, and apoptosis of cells, especially in cancer cells.[5] Altogether, nucleolin biological function contributes to cell homeostasis, and it has been identified that nucleolin is overexpressed in different cancer cell lines. Nucleolin overexpression contributes to tumorigenesis and cancer progression by potentiating a high level of protein synthesis, which supports cancer cell proliferation and survival. Nucleolin also promotes oncogenesis, acting as a transcriptional factor through direct binding to the promoter region of target genes in the nucleoplasm or by regulating the expression of several key proteins involved in cancer growth and progression at the cytoplasmic mRNA level. Christian et al. indicated that a cell surface nucleolin antagonist causes endothelial cell apoptosis and normalization of tumor vasculature.[6] Thus, a sensitivity technology for nucleolin detection is meaningful for tumor diagnosis and therapy.

Previous studies on nucleolin detection by traditional electrochemiluminescence (ECL) technology were primarily at the cell group level. Motaghi et al. employed a closed bipolar electrode system modified with the AS1411 aptamer integrated with ECL detection for sensitive diagnosis of nucleolin in human breast cancer cells.[7] However, ECL imaging is a powerful technique, which possesses many potential advantages combining chemiluminescence, electrochemistry, and imaging technology.[8−13] ECL imaging technology is increasingly being used to offer visual details of a single cell and single particle because it features the merits of low background and good temporal and spatial resolution. For example, Ding et al. explored ECL microscopy for imaging single living PC12 cell−matrix adhesions. This study makes ECL microscopy promising for studying the molecular composition, morphology, and mechanical properties of adhesions.[14] Although the ECL imaging method was used for a single cell or single nanoparticle study, the works on the integration of nucleolin diagnosis and therapy for tumor based on an ECL biosensor are still pretty rare.

Specific nanostructures that enable targeted and triggered release of signal tags and chemotherapeutic drugs are ideal for combined tumor diagnosis and therapy. Mesoporous silica nanoparticles (MSN) are nano-inorganic materials with a porous structure, which has the advantages of a large specific surface area, large loading capacity, and versatility of surface chemistry. Lately, MSN have been demonstrated to be efficient carriers of signal tags and chemotherapeutic drugs for targeted and triggered delivery due to the hollow nanostructures. The

Received: February 14, 2020
Accepted: March 30, 2020
Published: March 30, 2020

https://dx.doi.org/10.1021/acssensors.0c00292
ACS Sens. 2020, 5, 1216–1222

Scheme 1. ECL Imaging of Nucleolin in a Single Tumor Cell and Synergetic Apoptosis of Tumor Based on the ECL Biosensor

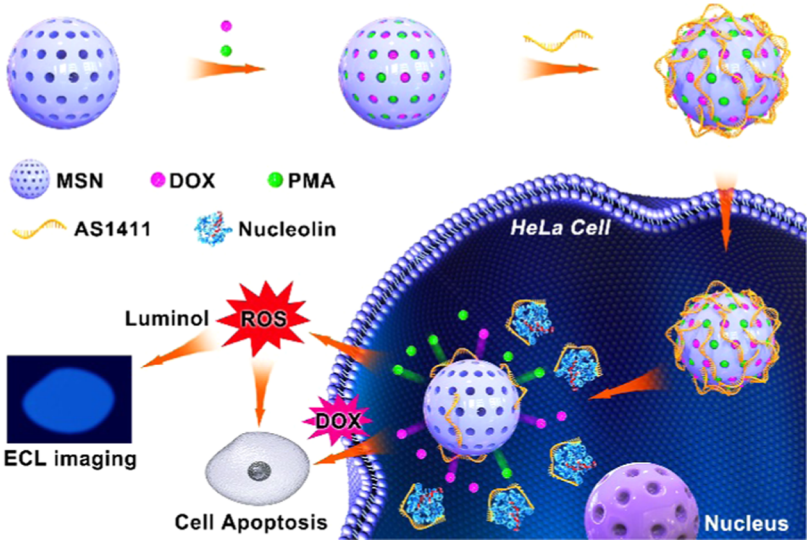

release process could not only potentially enable locoregional therapy but also avoid systemic toxicity of aggressive chemotherapeutic drugs.[15−19] In this article, MSN was chosen as a carrier for phorbol 12-myristate 13-acetate (PMA) and doxorubicin (DOX) to get a multifunctional MSN@PMA@DOX probe. DOX is a commonly used broad-spectrum antitumor drug, which causes tumor cell apoptosis mainly by inhibiting genetic material, nucleic acid, synthesis.[20−22] DOX has a good therapeutic effect on leukemia, lung tumor, ovarian tumor, breast tumor, and other tumors. Unlike DOX, PMA is a phorbol ester that stimulates tumor cells to produce reactive oxygen species (ROS).[23−26] High concentrations of ROS can damage the DNA and proteins of tumor cells, triggering oxidative stress-induced tumor cell death.[27−33] Before loading the drug, MSN was modified with 3-aminopropyltriethoxysilane (APTES) to have a positive charge on the surface. As the charge of AS1411 DNA was negative, MSN and AS1411 DNA were combined by electrostatic attraction. The MSN@PMA@DOX probe was finally closed by AS1411 DNA, which can specifically target nucleolin with high affinity (Scheme 1). After HeLa cells endocytosed the designed probe, AS1411 DNA could specifically combined with nucleolin with high binding force, which caused the AS1411 DNA to fall off the surface of MSN@PMA@DOX and targeted release of PMA and DOX. PMA stimulated tumor cells to produce ROS (including $O^{2-\bullet}$, $^{\bullet}OH$, H_2O_2, etc.), and H_2O_2 in ROS could react with luminol to produce an ECL signal, which was collected by the electron-multiplying charge-coupled device (EMCCD), and ECL images of nucleolin in HeLa cells were obtained. After that, HeLa cells could be killed with high efficiency due to the different apoptotic pathways of DOX and PMA. Herein, an ECL biosensor combining ECL imaging of nucleolin and synergetic therapy for tumor was established.

EXPERIMENTAL SECTION

Chemicals and Instrument. Doxorubicin (DOX), phorbol 12-myristate 13-acetate (PMA, 99%), and luminol were obtained from Sigma-Aldrich Inc. Phosphate-buffered saline (PBS, 0.1 M, pH 7.4) containing K_2HPO_4 and KH_2PO_4 was purchased from Beijing Solarbio Technology Co., Ltd. for dispersing the MSN probe. 3-Aminopropyltriethoxysilane (APTES) was purchased from Sinopharm Chemical Reagent Beijing Co., Ltd. (China). Cell Counting Kit-8 (CCK-8) was obtained from DOJINDO Laboratories (Shanghai, China). Annexin V-FITC/PI Apoptosis Detection Kit and Annexin V-EGFP/PI Apoptosis Detection Kit were purchased from Shanghai Yeasen. Fluorine-doped tin oxide (FTO)-coated glass was purchased from Kaivo (Zhuhai, China). All aqueous solutions were prepared using RNA-free water. DNA was purchased from Sangon Biotech (Shanghai, China) with the following sequences:

AS1411 5′-NH_2-C_6GGG GGG TTG GTG GTG GTG GTT GTG GTG GTG GTG G-3′

The CCK-8 assay was performed on an ultramicro microporous plate spectrophotometer (EP0CH2). The cell apoptosis images were obtained on a TCS SP8 II laser confocal microscope (Nikon C2plus, Germany) and using flow cytometry (Cytoflex, A00-1-1102). Transmission electron microscopy (TEM) images were obtained from a JEM-2100 microscope (Hitachi, Japan). ECL imaging was performed using a fluorescence inversion microscopy system (Nikon, Ti-U), an EMCCD (Andor, DU-897U-CS0), and a spectrograph (Andor, SR-500i-A). Dynamic light scattering (DLS) characterization analysis was performed on Malvern Zetasizer Nano ZS90 (U.K.).

Synthesis of the MSN@PMA@DOX Probe. The synthesis process of MSN is adopted from the previous report.[34] One milliliter of APTES was added to 100 mL of ethanol containing 1.0000 g of MSN, and the mixture was continuously stirred at 36 °C for 6 h. After centrifugation with ethanol, it was dried at 60 °C to obtain APTES-MSN. PMA (0.05 mL, 5 μg mL^{-1}) and DOX (0.05 mL, 0.25 mg mL^{-1}) were added to the suspension, stirred at room temperature overnight, centrifuged, and washed under vacuum to obtain MSN@PMA@DOX powder. One milligram of MSN@PMA@DOX and AS1411 DNA (50 μL, 10 μM) each was dispersed in 1 mL of PBS (1 mg mL^{-1}) and stirred at 37 °C for 1 h. After centrifugation, it was dispersed in PBS to obtain AS1411-closed MSN@PMA@DOX probes. Finally, the MSN@PMA@DOX probe obtained was stored at 4 °C in the dark.

Optimal Experimental Conditions. The incubation time of HeLa cells with the MSN@PMA@DOX probe and the concentration of luminol were optimized to get the best ECL imaging of nucleolin. HeLa cells were incubated with the MSN@PMA@DOX probe (1 mg mL^{-1}) for 0.5, 1, 1.5, and 2 h under the same concentration of luminol. Then, HeLa cells were detected with 0.01, 0.05, 0.1, and 1 mM luminol under the same incubation time with the MSN@PMA@DOX probe (1 mg mL^{-1}). The ECL signal was recorded with a chemiluminescent analytical and a MPI-E multifunctional electrochemical system.

https://dx.doi.org/10.1021/acssensors.0c00292
ACS Sens. 2020, 5, 1216−1222

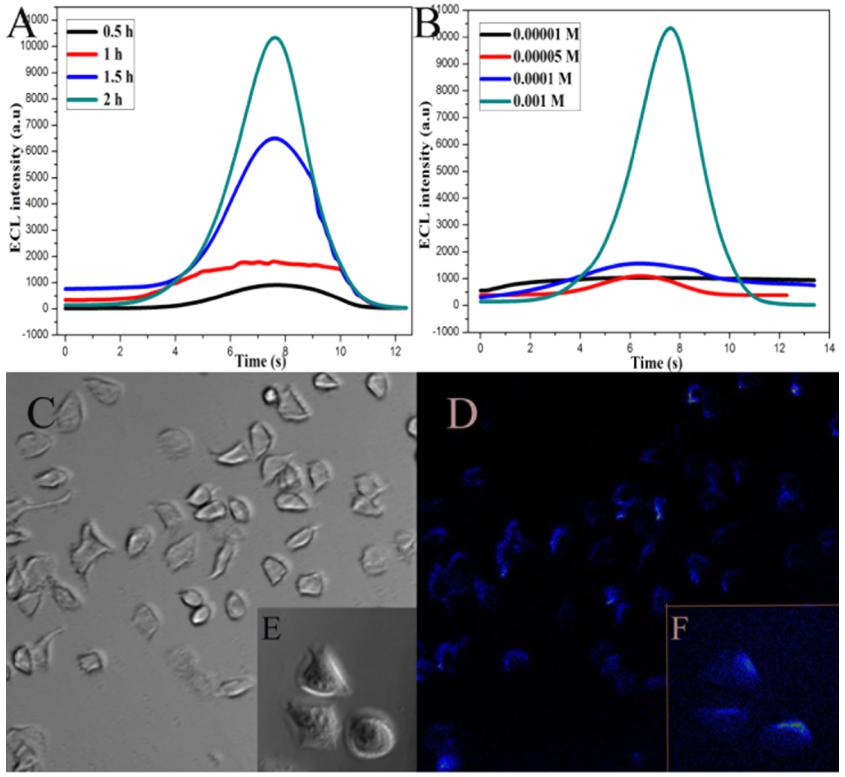

Figure 1. Plot of the ECL intensities vs (A) incubation time and (B) concentration of luminol. (C) HeLa cells' bright-field image. (D) HeLa cells' ECL image. (E) HeLa cells' amplified bright-field image. (F) HeLa cells' amplified ECL image on the FTO electrode chip; cells were incubated with the MSN@PMA@DOX probe; then, ECL images were recorded by EMCCD.

Manufacturing of the FTO Electrode Chip and the ECL Biosensor for Nucleolin Imaging in a Single Cell. The manufacturing process of the FTO electrode chip is adopted form the previous report.[33] FTO, a piece of 3.5 cm × 3 cm quartz glass, was modified with a special surface. The FTO chip was cleaned and sterilized for single-cell nucleolin imaging. Two cells with a diameter of 0.3 cm were punched at the central part of the poly-(dimethylsiloxane) (PDMS) layer as reservoirs. Afterward, the PDMS layer was attached to the FTO surface and pressed firmly. Then, the FTO electrode chip was manufactured. Based on the optimal experimental conditions, the MSN@PMA@DOX probe was incubated with cells on the chip for 2 h at 37 °C. Then, 20 μL of luminol solution (0.001 M, 0.01 M KOH, 1× PBS) was added to the detected cells, and by supplying 2.5 V, ECL imaging was performed by EMCCD. At the time of image acquisition, the focal plane was set to live cells and remained unchanged.

Cytotoxicity Experiments. HeLa cells (10 μL, 2.0 × 10^6 cells mL^{-1}) and LO-2 cells (10 μL, 2.0 × 10^6 cells mL^{-1}) were incubated with 6 μL of MSN, MSN@PMA, MSN@DOX, and MSN@PMA@DOX probes for 2, 4, 6, 8, 10, 12, and 24 h. Then, 10 μL of CCK-8 (5 mg mL^{-1}) was added to each well and protected from light in the incubator for 1 h at 37 °C. The absorbance of each well was measured at 450 nm by a microplate reader. Then, the cell viability was obtained using the following formula: cell viability (%) = $[(A_{test} - A_{blank})/(A_{control} - A_{blank})] \times 100\%$,.

Synergetic Apoptosis Study. HeLa cells (0.2 mL, 1 × 10^6 cells mL^{-1}) were reacted with MSN MSN@PMA@DOX, MSN@PMA, and MSN@DOX probes for 24 h, respectively. LO-2 cells (0.2 mL, 1 × 10^6 cells mL^{-1}) were reacted with MSN@PMA, MSN@DOX, and MSN@PMA@DOX probes for 24 h. Cell apoptosis rates were quantified by flow cytometry and detected by the Annexin V-FITC/PI Apoptosis Detection Kit. The experiment was performed according to the kit instructions. The cells in the early apoptosis stage were negative for PI but positive for Annexin V-FITC, the cells at late-stage apoptosis were stained by both PI and Annexin V-FITC. Laser confocal microscopy detection by the Annexin V-EGFP/PI Apoptosis Detection Kit further validated the synergetic apoptosis of PMA and DOX. The experiment was performed according to the kit instructions.

RESULTS AND DISCUSSION

ECL Biosensor for Nucleolin Imaging in a Single Tumor Cell. To make sure the ECL biosensor can optimize the analysis performance of nucleolin, the influence of incubation time for the MSN@PMA@DOX probe and HeLa cells and the concentration of luminol was studied and is shown in Figure 1. The curves in Figure 1A show that the ECL intensity of the HeLa cells gradually increased with the increasing incubation time and the maximum signal strength was reached at 2 h. This phenomenon may be attributed to the time taken by cells to endocytose probes and to generate ROS upon PMA stimulation. From Figure 1B, we can observe that the ECL intensity of HeLa cells increased with the increasing concentration of luminol, which is in accordance with the mechanism of the ECL system for luminol and H_2O_2, and the concentration of luminol of 1 mM can produce the maximum ECL intensity. Therefore, considering the preferable stability and ECL intensity, the ECL biosensor was used under the conditions of incubation time of 2 h and the concentration of luminol of 1 mM. The image in Figure 1C shows the morphology of HeLa cells. The ECL imaging of nucleolin in a single HeLa cell was performed by EMCCD under the conditions of 2 h incubation time and 1 mM concentration of luminol solution (Figure 1D). The amplified bright-field imaging of HeLa cells is shown in Figure 1E, and the amplified ECL imaging of nucleolin is shown in Figure 1F. This phenomenon could be attributed to the high activity of nucleolin in HeLa cells, which could bind with the AS1411

https://dx.doi.org/10.1021/acssensors.0c00292
ACS Sens. 2020, 5, 1216−1222

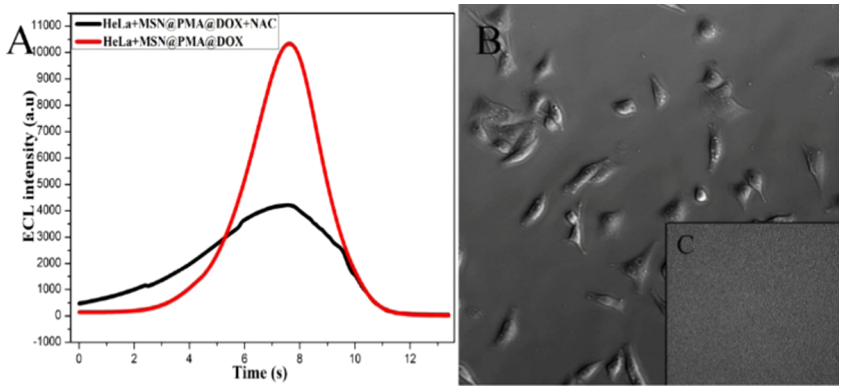

Figure 2. (A) Plot of the ECL intensities vs reactive oxygen species scavenger. (B) LO-2 cells' bright-field image. (C) LO-2 cells' ECL image on the FTO electrode chip; cells were incubated with the MSN@PMA@DOX probe; then, ECL images were recorded by EMCCD.

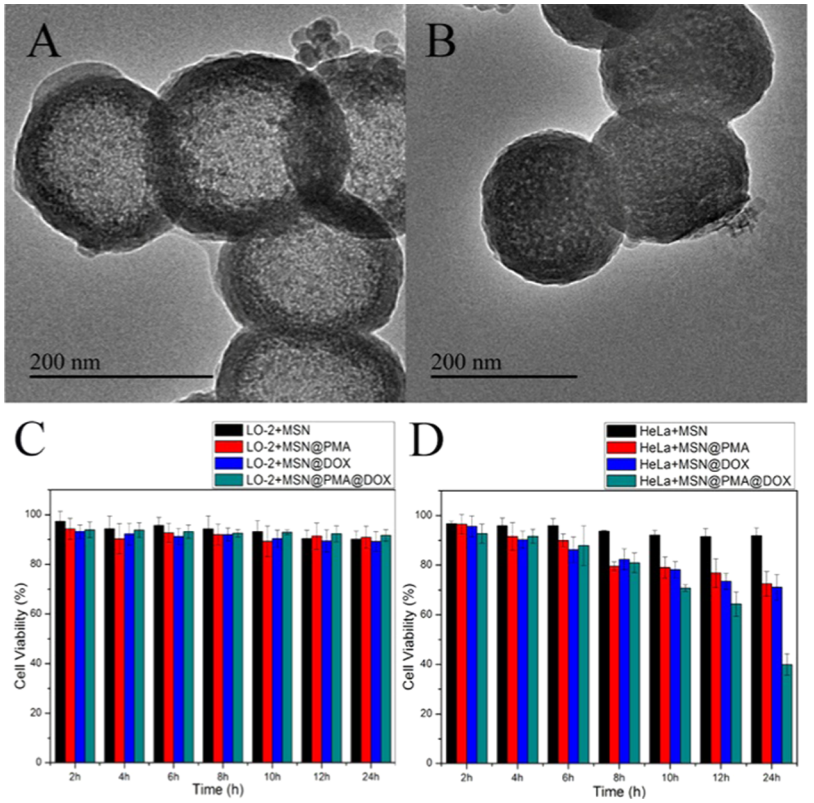

Figure 3. Transmission electron microscopy (TEM) image of synthesized (A) MSN and (B) AS1411 DNA sealing the MSN@PMA@DOX probe. Viability of (C) LO-2 cells and (D) HeLa cells incubated with MSN, MSN@PMA, MSN@DOX, and MSN@PMA@DOX probes.

aptamer and release PMA from the MSN@PMA@DOX probe. The released PMA could lead to increased intracellular ROS levels of HeLa cells. H_2O_2, one of the molecules in ROS, could react with luminol at a certain voltage to produce the ECL signal. The ECL signal was finally acquired by EMCCD and transformed into ECL imaging of nucleolin.

After adding a reactive oxygen species scavenger, there was a lower ECL signal than that from the test group of HeLa cells (Figure 2A). This phenomenon showed that the ECL signal was produced by H_2O_2 and luminol at a certain voltage. The released PMA stimulated tumor cells to produce ROS (including $O^{2-\bullet}$, $^{\bullet}OH$, H_2O_2, etc.). However, the intensity of the ECL signal decreased after the addition of the reactive oxygen species scavenger NAC. Therefore, there was no or microscale ROS in the cells. Figure 2B is the bright-field image of LO-2 cells, and Figure 2C is the ECL image of LO-2 cells. It is worth noting that there is no ECL signal of LO-2 cells compared with HeLa cells under the same experimental conditions. This phenomenon shows that the MSN@PMA@DOX probe cannot be opened in normal cells without nucleolin. Therefore, the designed ECL biosensor can be specifically recognized by nucleolin in tumor cells and achieve tumor diagnosis and therapy.

Characterization and Cytotoxicity of the Drug Delivery System. The morphology of MSN was studied by transmission electron microscopy (TEM) to ensure high delivery efficiency of the built drug-loading system. The synthesized MSN showed equal size with an average diameter of about 180 nm, with a hollow and porous structure (Figure 3A). As shown in Figure 3B, after the MSN was filled with

https://dx.doi.org/10.1021/acssensors.0c00292
ACS Sens. 2020, 5, 1216−1222

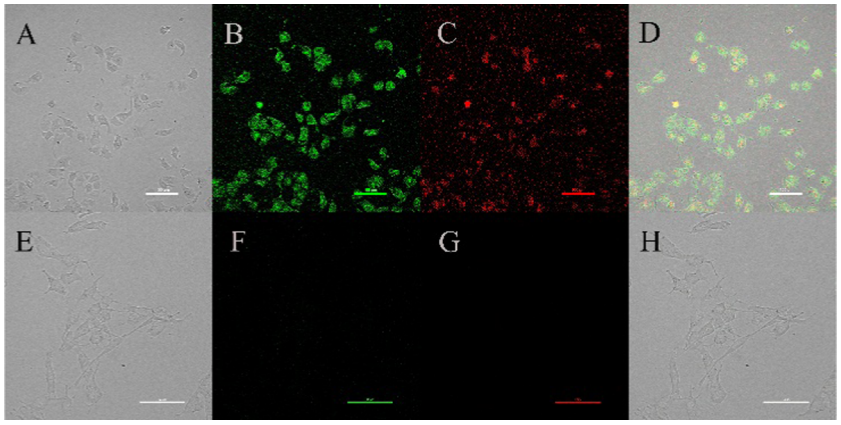

Figure 4. Confocal laser scanning microscopy (CLSM) images of HeLa cells and LO-2 cells after incubation with the MSN@PMA@DOX probe for 24 h. (A, E) Bright field provides cell information. (B, F) Early apoptotic cell information: the green channel was collected at 500−570 nm under excitation at 488 nm (fluorescent dye, Annexin V-EGFP). (C, G) Late apoptotic cell information: red channel was collected at 650−720 nm under excitation at 535 nm (fluorescent dye, PI). (D, H) Merged image: green channel, red channel, and bright field.

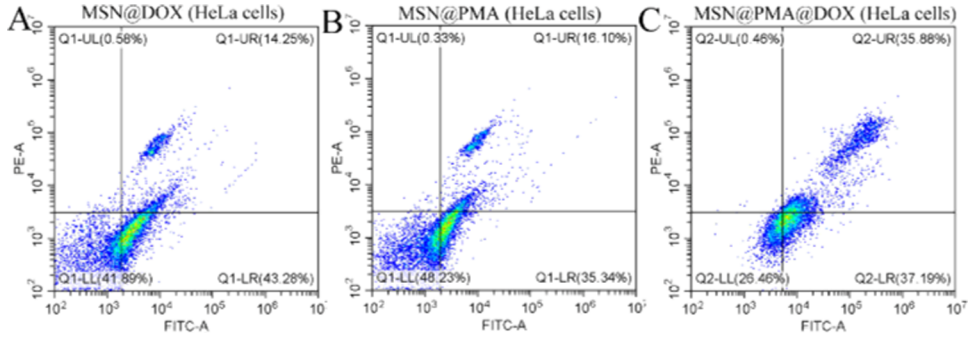

Figure 5. Flow cytometry study of HeLa cells treated with (A) MSN@DOX probe (1 mg mL^{-1}) for 24 h, (B) MSN@PMA probe (1 mg mL^{-1}) for 24 h, and (C) MSN@PMA@DOX probe (1 mg mL^{-1}) for 24 h; the cells were stained with the Annexin V-FITC/PI Apoptosis Detection Kit.

PMA and DOX and closed by the AS1411 aptamer, the MSN became darker, which means that the holes of the MSN were closed by the AS1411 aptamer and the MSN@PMA@DOX probe was successfully synthesized. The result of dynamic light scattering (DLS) in Figure S1 showed that the average diameter of the MSN and the MSN@PMA@DOX probe was consistent with TEM, about 180 nm. To evaluate whether the MSN probe is suitable for cancerous cell treatment, the biocompatibility of the MSN probe was tested by the CCK-8 assay. The viability of LO-2 cells after incubation with the MSN, MSN@PMA, MSN@DOX, and MSN@PMA@DOX probes was more than 90% (Figure 3C). As can be seen in Figure 3D, the HeLa cell survival rate when cultivated with MSN nanoparticles was more than 90%, which means that MSN was fully biocompatible to be used as a drug carrier and in tumor therapy. After cultivation with MSN@PMA and MSN@DOX probes for 24 h, the survival rate of HeLa cells was 72 and 71%, respectively. However, the HeLa cell survival rate after cultivation with the MSN@PMA@DOX probe for 24 h was less than 40%. The nucleolin in HeLa cells can bind to the AS1411 aptamer on the probe, which leads to the release of PMA and DOX inside the probe. Under the combination of PMA and DOX, HeLa cells are efficiently killed by the synergetic apoptosis pathway. The experimental results show that the designed probe is not cytotoxic to normal cells. This is mainly attributed to the AS1411 aptamer modified on the probe could not be opened as the nucleolin was not active in LO-2 or other normal cells.

Apoptosis of HeLa Cells. To study the therapeutic effect of HeLa cells, the apoptosis efficiency of HeLa cells can be observed by laser confocal microscopy. It was verified by confocal laser experiments with Annexin V-EGFP/PI staining that the MSN@PMA@DOX probe can induce hyperapoptosis in HeLa cells. As shown in Figure 4, early apoptotic HeLa cells were stained with Annexin V-EGFP and collected at 488 nm for green fluorescence imaging at 500−570 nm to obtain cell information at an early apoptotic stage (Figure 4B). In addition, to obtain late apoptotic cell information, late apoptotic HeLa cells were double-stained with Annexin V-EGFP and PI, and red fluorescence imaging was performed at 650−720 nm under excitation at 535 nm (Figure 4C). It can be seen through comparative experiments that the MSN@PMA@DOX probe can target and effectively kill tumor cells without damage to normal somatic cells (Figure 4F−H). Flow cytometry further quantifies the therapeutic effect of the drug system. It can be seen in the Supporting Information that, after incubation with MSN, 4.41% of HeLa cells were in apoptosis (Figure S2A). This further verified that MSN has good biocompatibility. Flow cytometry results of LO-2 cells incubated with the MSN@PMA@DOX, MSN@PMA, and MSN@DOX probes show that 2.62, 3.49, and 2.96% of LO-2 cells were in the apoptotic stage, respectively (Figure S2B−D). This means that the probe only targeted HeLa cells. The flow cytometry result of HeLa cells incubated with MSN@DOX and MSN@PMA probes shows that 57.53% and 51.44% of HeLa cells were in the apoptosis stage, respectively (Figure

https://dx.doi.org/10.1021/acssensors.0c00292
ACS Sens. 2020, 5, 1216−1222

5A,B). Figure 5C shows that 73.07% of HeLa cells were in the apoptosis stage after incubation with the MSN@PMA@DOX probe for 24 h, which was significantly higher than that of the single probe group. The pathway of DOX to cause HeLa cell apoptosis was inhibition of genetic material, nucleic acid, synthesis. However, PMA stimulated HeLa cells to produce high concentrations of ROS to damage the DNA and proteins of the cells. Under the combination of PMA and DOX, the synergetic apoptosis pathway of the MSN@PMA@DOX probe can target and effectively kill HeLa cells without damage to normal somatic cells.

CONCLUSIONS

In this work, the ECL biosensor and the MSN@PMA@DOX probe were used for nucleolin diagnosis in a single HeLa cell and synergetic therapy of tumors. Compared with previous studies, this work provides a new method that studies nucleolin imaging in a single HeLa cell by an ECL biosensor with high sensitivity and low cost. Besides, the built synergetic apoptosis pathway by PMA and DOX could induce highly specific apoptosis of the HeLa cell. More importantly, the integration of tumor diagnosis and therapy provides a theoretical foundation for clinical applications.

ASSOCIATED CONTENT

Supporting Information

The Supporting Information is available free of charge at https://pubs.acs.org/doi/10.1021/acssensors.0c00292.

DLS characterization analysis of MSN and MSN@PMA@DOX probes; flow cytometry study of HeLa cells and LO-2 cells (PDF)

AUTHOR INFORMATION

Corresponding Authors

Huairong Zhang − *Shandong Sino-Japanese Center for Collaborative Research of Carbon Nanomaterials, College of Chemistry and Chemical Engineering, Qingdao University, Qingdao, Shandong 266071, China; Collaborative Innovation Center of Tumor Marker Detection Technology, Equipment and Diagnosis-Therapy Integration in Universities of Shandong, Shandong Province Key Laboratory of Detection Technology for Tumor Makers, School of Chemistry and Chemical Engineering, Linyi University, Linyi 276005, China;* orcid.org/0000-0003-3420-8005; Email: zhanghuairong999@126.com

Zonghua Wang − *Shandong Sino-Japanese Center for Collaborative Research of Carbon Nanomaterials, College of Chemistry and Chemical Engineering, Qingdao University, Qingdao, Shandong 266071, China*; Email: 13853219173@126.com

Authors

Wanxia Gao − *Shandong Sino-Japanese Center for Collaborative Research of Carbon Nanomaterials, College of Chemistry and Chemical Engineering, Qingdao University, Qingdao, Shandong 266071, China; Collaborative Innovation Center of Tumor Marker Detection Technology, Equipment and Diagnosis-Therapy Integration in Universities of Shandong, Shandong Province Key Laboratory of Detection Technology for Tumor Makers, School of Chemistry and Chemical Engineering, Linyi University, Linyi 276005, China*

Yong Liu − *Collaborative Innovation Center of Tumor Marker Detection Technology, Equipment and Diagnosis-Therapy Integration in Universities of Shandong, Shandong Province Key Laboratory of Detection Technology for Tumor Makers, School of Chemistry and Chemical Engineering, Linyi University, Linyi 276005, China*

Complete contact information is available at: https://pubs.acs.org/10.1021/acssensors.0c00292

Notes

The authors declare no competing financial interest.

ACKNOWLEDGMENTS

This work was supported by the National Natural Science Foundation of China (21605069), the China Postdoctoral Science Foundation (2016M600518), and the Taishan Scholar Foundation of Shandong Province (ZR2017ZC0226).

REFERENCES

(1) Li, N.; Yuan, K.; Yan, F.; Huo, Y.; Zhu, T.; Liu, X.; Guo, Z.; Yao, X. B. PinX1 is recruited to the mitotic chromosome periphery by Nucleolin and facilitates chromosome congression. *Biochem. Biophys. Res. Commun.* **2009**, *384*, 76−81.

(2) Lee, J. H.; Lee, Y. S.; Jeong, S. A.; Khadka, P.; Roth, J.; Chung, I. K. Catalytically active telomerase holoenzyme is assembled in the dense fibrillar component of the nucleolus during S phase. *Histochem. Cell Biol.* **2014**, *141*, 137−152.

(3) Wen, S. P.; Miao, X. R.; Fan, G.-C.; Xu, T. T.; Jiang, L.-P.; Wu, P.; Cai, C. X.; Zhu, J.-J. Aptamer-Conjugated Au Nanocage/SiO_2 Core-Shell Bifunctional Nanoprobes with High Stability and Biocompatibility for Cellular SERS Imaging and Near-Infrared Photothermal Therapy. *ACS Sens.* **2019**, *4*, 301−308.

(4) Shen, L.; Bing, T.; Zhang, N.; Wang, L. L.; Wang, J. Y.; Liu, X. J.; Shang guan, D. H. A Nucleus-Targeting DNA Aptamer for Dead Cell Indication. *ACS Sens.* **2019**, *4*, 1612−1618.

(5) Cao, C. Y.; Wei, P.; Li, R. H.; Zhong, Y. P.; Li, X.; Xue, F. F.; Shi, Y. B.; Yi, T. Ribosomal RNA-Selective Light-Up Fluorescent Probe for Rapidly Imaging the Nucleolus in Live Cells. *ACS Sens.* **2019**, *4*, 1409−1416.

(6) Fogal, V.; Sugahara, K. N.; Ruoslahti, E.; Christian, S. Cell surface nucleolin antagonist causes endothelial cell apoptosis and normalization of tumor vasculature. *Angiogenesis* **2009**, *12*, 91−100.

(7) Motaghi, H.; Ziyaee, S.; Mehrgardi, M. A.; Kajani, A. A.; Bordbar, A.-K. Electrochemiluminescence detection of human breast cancer cells using aptamer modified bipolar electrode mounted into 3D printed microchannel. *Biosens. Bioelectron.* **2018**, *118*, 217−223.

(8) Zhang, J.-D.; Lu, L.; Zhu, X.-F.; Zhang, L.-J.; Yun, S.; Duanmu, C.-S.; He, L. Direct observation of oxidation reaction via closed bipolar electrode-anodic electrochemiluminescence protocol: structural property and sensing applications. *ACS Sens.* **2018**, *3*, 2351−2358.

(9) Bishop, G. W.; Satterwhite-Warden, J. E.; Bist, I.; Chen, E.; Rusling, J. F. Electrochemiluminescence at bare and DNA-coated graphite electrodes in 3D-printed fluidic devices. *ACS Sens.* **2016**, *1*, 197−202.

(10) Feng, X.; Han, T.; Xiong, Y. F.; Wang, S. C.; Dai, T. Y.; Chen, J. H.; Zhang, X. J.; Wang, G. F. Plasmonenhanced electrochemiluminescence of silver nanoclusters for microRNA detection. *ACS Sens.* **2019**, *4*, 1633−1640.

(11) Zhang, J. J.; Zhou, J. Y.; Pan, R. R.; Jiang, D. C.; Burgess, J. D.; Chen, H.-Y. New frontiers and challenges for single-cell electrochemical analysis. *ACS Sens.* **2018**, *3*, 242−250.

(12) Zhang, H.-R.; Wu, M.-S.; Xu, J.-J.; Chen, H.-Y. Signal-on dual-potential electrochemiluminescence based on luminol-gold bi-functional nanoparticles for telomerase detection. *Anal. Chem.* **2014**, *86*, 3834−3840.

(13) Xu, H. Y.; Zhou, S.; Jiang, D. C.; Chen, H.-Y. Cholesterol oxidase/triton X-100 parked microelectrodes for the detection of

cholesterol in plasma membrane at single cells. *Anal. Chem.* **2018**, *90*, 1054−1058.
(14) Ding, H.; Guo, W. L.; Su, B. Imaging cell-matrix adhensions and collective migration of living cells by electrochemiluminescence microscopy. *Angew. Chem.* **2020**, *132*, 457−464.
(15) Nasir, T.; Herzog, G.; Hebrant, M.; Despas, C.; Liu, L.; Walcarius, A. Mesoporous Silica Thin Films for Improved Electrochemical Detection of Paraquat. *ACS Sens.* **2018**, *3*, 484−493.
(16) Gu, Z. F.; Fu, A. C.; Ye, L.; Kuerban, K.; Wang, Y.; Cao, Z. J. Ultrasensitive Chemiluminescence Biosensor for Nuclease and Bacterial Determination Based on Hemin-Encapsulated Mesoporous Silica Nanoparticles. *ACS Sens.* **2019**, *4*, 2922−2929.
(17) Wang, L. M.; Zhu, F. W.; Chen, M.; Xiong, Y.; Zhu, Y. Q.; Xie, S. Q.; Liu, Q.; Yang, H.; Chen, X. Q. Development of a "Dual Gates" Locked, Target-Triggered Nanodevice for Point-of-Care Testing with a Glucometer Readout. *ACS Sens.* **2019**, *4*, 968−976.
(18) Hubbell, J. A.; Chilkoti, A. Nanomaterials for drug delivery. *Science* **2012**, *337*, 303−305.
(19) Allen, T. M.; Cullis, P. R. Drug delivery systems: entering the main stream. *Science* **2004**, *303*, 1818−1822.
(20) Wang, F. C.; Li, Q.; Zhang, P. J.; Liu, X. H.; Li, A.; Yang, J.; Liu, D. B. Assembly of DNA Probes into Superstructures for Dramatically Enhancing Enzymatic Stability and Signal-to-Background Ratio. *ACS Sens.* **2018**, *3*, 2702−2708.
(21) Shaibani, P. M.; Etayash, H.; Naicker, S.; Kaur, K.; Thundat, T. Metabolic Study of Cancer Cells Using a pH Sensitive Hydrogel Nanofiber Light Addressable Potentiometric Sensor. *ACS Sens.* **2017**, *2*, 151−156.
(22) Wong, R. C. H.; Ng, D. K. P.; Fong, W.-P.; Lo, P.-C. Encapsulating phresponsive doxorubicin-phthalocyanine conjugates in mesoporous silica nanoparticles for combined photodynamic therapy and controlled chemotherapy. *Chem. - Eur. J.* **2017**, *23*, 16505−16515.
(23) Gongol, B.; Marin, T.; Shyy, J. Abstract 446: ampk regulates endo thelial mirna biogenesis through nucleolin. *Arterioscler., Thromb., Vasc. Biol.* **2019**, *38*, A446.
(24) Javor, K.; Tisserant, J.-N.; Stemmer, A. Biofuel cell operating on activated THP-1 cells: a fuel and substrate study. *Biosens. Bioelectron.* **2017**, *87*, 1−6.
(25) Lu, X. H.; Chen, Z. J.; Dong, X. C.; Zhao, W. L. Water-Soluble Fluorescent Probe with Dual Mitochondria/Lysosome Targetability for Selective Superoxide Detection in Live Cells and in Zebrafish Embryos. *ACS Sens.* **2018**, *3*, 59−64.
(26) Rodriguez-Moncayo, R.; Jimenez-Valdes, R. J.; Gonzalez-Suarez, A. M.; Garcia-Cordero, J. L. Integrated Microfluidic Device for Functional Secretory Immunophenotyping of Immune Cells. *ACS Sens.* **2020**, *5*, 353−361.
(27) Higashi, Y.; Mazumder, J.; Yoshikawa, H.; Saito, M.; Tamiya, E. Chemically regulated ROS generation from gold nanoparticles for enzyme-free electrochemiluminescent immunosensing. *Anal. Chem.* **2018**, *90*, 5773−5780.
(28) Hicks, J. M.; Halkerston, R.; Silman, N.; Jackson, S. K.; Aylotta, J. W.; Rawson, F. J. Real-time bacterial detection with an intracellular ROS sensing platform. *Biosens. Bioelectron.* **2019**, *141*, No. 111430.
(29) Dai, Y. P.; He, F. R.; Ji, H. F.; Zhao, X. X.; Misal, S.; Qi, Z. J. Dual-functional N. I. R. AIEgens for high-fidelity imaging of lysosomes in cells and photodynamic therapy. *ACS Sens.* **2020**, *5*, 225−233.
(30) Ozel, R. E.; Bulbul, G.; Perez, J.; Pourmand, N. Functionalized Quartz Nanopipette for Intracellular Superoxide Sensing: A Tool for Monitoring Reactive Oxygen Species Levels in Single Living Cell. *ACS Sens.* **2018**, *3*, 1316−1321.
(31) Zhang, Z.; Fan, J. L.; Zhao, Y. H.; Kang, Y.; Du, J. J.; Peng, X. J. Mitochondria-Accessing Ratiometric Fluorescent Probe for Imaging Endogenous Superoxide Anion in Live Cells and Daphnia magna. *ACS Sens.* **2018**, *3*, 735−741.
(32) Stanicka, J.; Russell, E. G.; Woolley, J. F.; Cotter, T. G. NADPH ox idase-generated hydrogen peroxide induces DNA damage in mutant FLT3-expressing leukemia cells. *J. Biol. Chem.* **2015**, *290*, 9348−9361.
(33) Zhang, H. R.; Gao, W. X.; Liu, Y.; Sun, Y. N.; Jiang, Y. X. L.; Zhang, S. S. Electrochemiluminescence-microscopy for microRNA imaging in single cancer cell combined with chemotherapy-photothermal therapy. *Anal. Chem.* **2019**, *91*, 12581−12586.
(34) Wu, S.-H.; Mou, C.-Y.; Lin, H.-P. Synthesis of mesoporous silica nanoparticles. *Chem. Soc. Rev.* **2013**, *42*, 3862−3875.

https://dx.doi.org/10.1021/acssensors.0c00292
ACS Sens. 2020, 5, 1216−1222